

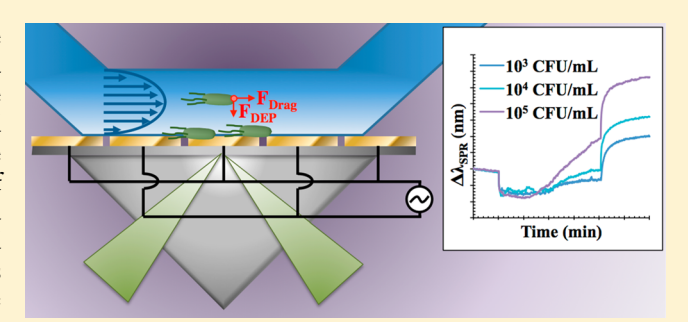
# Sensitive Bacterial Detection via Dielectrophoretic-Enhanced Mass Transport Using Surface-Plasmon-Resonance Biosensors

Daniel David Galvan, Vidit Parekh, Erik Liu, E-Lin Liu, and Qiuming Yu\*

Department of Chemical Engineering, University of Washington, Seattle, Washington 98195, United States

Supporting Information

**ABSTRACT:** The performance of surface plasmon resonance (SPR)-based bacterial biosensors is often compromised as a result of diffusion-limited mass transport of bacteria to the sensing surface. In this work, dually functional interdigitated electrodes (IDEs) were developed to sustain SPR and increase bacterial mass transport through external application of dielectrophoresis (DEP). IDEs were defined into 50 nm Au films with fixed electrode gaps ( $E_{\rm G}=5~\mu{\rm m}$ ) and varied electrode widths ( $E_{\rm W}=10$ , 20, and 100  $\mu{\rm m}$ ), referred to as interdigitated SPR (iSPR) chips. The iSPR chips with  $E_{\rm W}=100~\mu{\rm m}$  effectively supported SPR, with comparable sensitivity



to those of conventional SPR chips. The surfaces of iSPR chips ( $E_{\rm W}=100~\mu{\rm m}$ ) were modified with mannose to target the FimH adhesin of *Escherichia coli* and increase cellular adhesion. An LOD of  $\sim 3.0 \times 10^2$  CFU/mL *E. coli* was achieved on mannosylated iSPR chips under positive-DEP conditions, which is about a 5 order of magnitude improvement compared with those of mannosylated conventional SPR chips without DEP. Furthermore, secondary antibody amplification enabled selective enhancement of dilute ( $10^3$  CFU/mL) *E. coli* suspensions, whereas no amplification was observed for concentrated ( $10^8$  CFU/mL) nontarget ( $10^8$  CFU/mL) bacterial suspensions. The results presented here indicate the great potential of the incorporation of DEP into SPR biosensors for rapid, sensitive, and specific detection of bacteria with broad applications in areas of biomedical diagnostics, environmental monitoring, food safety, and homeland security.

B acterial infections are commonplace worldwide. The increased prevalence of bacterial infections has resulted in the over prescription of wide-spectrum antibiotics, and a dramatic decrease in the efficiency of antibiotic treatment. <sup>1,2</sup> In the United States alone, ~2 million cases of bacterial infections exhibiting some degree of antibiotic resistance are reported annually, resulting in ~23 000 deaths.<sup>3-5</sup> Diagnosis of bacterial infections is predominately performed by time-consuming and expensive plate-culturing methods. The relatively dilute concentrations at which bacteria are present in clinical samples further complicate diagnoses. For example, a positive urinarytract infection is defined as a bacterial concentration <10<sup>5</sup> CFU/mL, and complications in the collection process can reduce the concentration to 10<sup>3</sup> CFU/mL. The development of novel technologies is required to reduce diagnosis times and thus alleviate antibiotic pressure on bacteria leading to resistance.

Surface plasmon resonance (SPR) is one such biosensing technology that is well suited for bacterial detection. SPR-based biosensing capitalizes on the coupling of incident light to surface plasmons (SPs) on metal—dielectric interfaces. SPs are generated when the momentum of the electric component of incident light matches that of the free-electron plasma of the metal. Two critical lengths define the SPs and how they interact with the surrounding dielectric environment: the propagation length, which is the average distance SPs propagate along the metal—dielectric interface, and the

penetration depth, the distance above the metal–dielectric interface at which the SP-electric-field intensity decays by a factor of 1/e. While both characteristic lengths are dependent on the specific excitation wavelength, metal-film properties, and dielectric medium, typical ranges for the propagation length and penetration depth in the 650–830 nm spectral window are 3–20  $\mu m$  and 162–400 nm, respectively.  $^{10}$  SPs are sensitive to the dielectric environment near the interface. Local changes in the refractive index of the medium directly above the metal–dielectric interface induce shifts in the SPR wavelength, and with a proper experimental setup the SPR-wavelength shift can indicate a specific biorecognition event (e.g., adsorption of bacteria on the surface). The magnitude of the shift can be used to quantify the concentration and identify the target bacteria.

The performance of SPR bacterial biosensors is directly related to the efficiency at which bacterial cells are brought into the effective sensing volume of the SP evanescent wave. SPR biosensing can suffer from undesirably high limits of detection (LODs) because of inherent performance limitations originating from (1) the  $\sim \! 300$  nm penetration depth and (2) diffusion-limited mass transport of bacterial cells to the metal—

Received: November 6, 2018
Accepted: November 15, 2018
Published: November 15, 2018

dielectric interface. Multiple strategies have been explored to improve LODs in SPR-based bacterial detection. Sandwichtype assays provide secondary amplification of the SPR signal through further alteration of the local dielectric environment and have been shown to improve the LOD. 11-13 Long-range SPR (LR-SPR) biosensors were developed to extend the penetration depth from ~300 nm to approximately the diameter of bacterial cells (~1  $\mu$ m). 14-16 Increased coverage of the bacterial cells by the LR-SPR evanescent wave led to 5.5-fold increase in SPR response for the detection of *Escherichia coli* HB101P. 14 However, most SPR bacterial biosensing is performed in microfluidic channels with a critical channel height of ~50  $\mu$ m. Therefore, the majority of the microchannel, and thus the bacterial cells, remain inaccessible to the SP evanescent wave, hindering detection performance.

SPR bacterial biosensors are often operated in a diffusionlimited regime, which can further limit device performance. Of the key kinetic processes that bacterial cells experience in the microchannel, which include convection through the length of the microchannel, diffusion from the bulk fluid to the sensing surface, and reaction at the sensing surface, diffusion is often the slowest process.<sup>17</sup> For dilute suspensions in the clinically relevant range (<10<sup>5</sup> CFU/mL), the majority of target cells transverse the microchannel without adsorption on the sensor surface. Therefore, it is desired to increase mass transport of bacterial cells to the metal-dielectric interface for efficient detection. Magnetic nanoparticles (MNPs) have been the predominant mechanism explored in SPR biosensing to increase bacterial mass transport. MNPs are typically functionalized with antibodies or aptamers to selectively bind the target cells, and application of an externally applied magnetic field drives mass transport of MNP-bacteria complexes to the sensing surface. One unexplored avenue that holds potential for overcoming diffusion-limited mass transport and improving LOD performance in SPR bacterial detection is dielectrophoresis (DEP).

DEP is the movement of dielectric particles (i.e., bacterial cells) in the presence of an asymmetrical electric field. <sup>21</sup> The dielectrophoretic force exerted on the particle is dependent on the size, shape, and permittivity of the particle; the conductivity of the suspending medium; the square electric-field gradient; and the frequency of the applied AC potential. <sup>22</sup> In the presence of inhomogeneous electric fields, particles will migrate toward regions where the electric-field gradient is maximized or minimized in positive DEP (pDEP) and negative DEP (nDEP), respectively. Properly designed DEP-active electrodes can therefore lead to biosensing-signal enhancement through spatial modulation of bacterial cells. DEP has been successfully incorporated into various bacterial-biosensing strategies, including electrochemical-impedance spectroscopy, <sup>23–26</sup> fluorescence microscopy, <sup>27–29</sup> Raman spectroscopy, <sup>30–32</sup> and surface-enhanced Raman scattering. <sup>33–36</sup>

Therefore, it was speculated that DEP could be incorporated into the SPR-sensing strategy to overcome diffusion-limited mass transport and increase bacterial-detection efficiency. In this work, we report the development of a DEP—SPR bacterial-detection technique with dually functional interdigitated electrodes (IDEs) on SPR chips, henceforth referred to as interdigitated-SPR chips (iSPR chips). The iSPR chips were optimized to sustain strong SPR, while simultaneously providing increased mass transport of bacterial cells to the sensing surface through DEP. SP generation was found to be dependent on electrode width, with efficient SP generation

occurring on IDEs with widths larger than the SP-propagation length. The inherent sensitivity to bulk changes in the refractive index of the sensing medium for the iSPR chip was compared against that of a conventional (i.e., continuous Au film) SPR chip. The two types of SPR chips generated nearly identical SPR shifts for changes in the refractive index of 0.001 25 RIU. Conventional- and iSPR-chip surfaces were functionalized with mannose to target the FimH adhesin of E. coli and increase cellular adhesion. The DEP-SPR method enabled a nearly 5 order of magnitude improvement in the LOD for E. coli suspensions compared with that of a conventional SPR biosensor, improving the LOD from 1.0  $\times$  $10^7$  CFU/mL to  $\sim 3.0 \times 10^2$  CFU/mL. Furthermore, selective detection of target E. coli over nontarget Staphylococcus epidermidis bacteria was enabled through secondary antibody amplification. The results presented here indicate a great potential of the incorporation of DEP into SPR biosensors for rapid, sensitive, and specific detection of bacteria with broad applications in the areas of biomedical diagnostics, environmental monitoring, food safety, and homeland security.

### MATERIALS AND METHODS

Chemicals and Reagents. Potassium hydroxide, potassium thiosulfate, potassium ferricyanide, potassium ferrocyanide, octadecanethiol (ODT), 11-mercaptoundecanoic acid (MUA), sodium chloride, tryptone, yeast extract, trichloro-(1H,1H,2H,2H-perfluorooctyl)silane (TCPFOS), 1-ethyl-3-[3-(dimethylamino)propyl]carbodiimide HCl (EDC), N-hydroxysuccinimide (NHS), and bovine-serum albumin (BSA) were purchased from Sigma-Aldrich. 1-Deoxy-1-aminomannopyranoside (DAMP) was purchased from Santa Cruz Biotechnology. Sylgard 184 polydimethylsiloxane (PDMS) and curingagent elastomer kit were purchased from Dow Corning. Escherichia coli (ATCC 25922) and Staphylococcus epidermidis (ATCC 14990) were purchased from American Type Culture Collection. Rabbit anti-E. coli polyclonal antibodies (PA1-7213) were purchased from Invitrogen. All chemicals were used as received.

Fabrication of iSPR Chips. iSPR chips were fabricated through a series of photolithography, soft-lithography, and chemical-etching steps. IDE patterns were first developed into a  $\sim$ 3  $\mu$ m SU-8 film on a silicon wafer using photolithography. Three patterns were resolved on the SU-8 master mold with a fixed electrode gap  $(E_G)$  of 5  $\mu$ m and electrode widths  $(E_W)$  of 10, 20, and 100  $\mu$ m. A detailed schematic for the electrode configurations can be seen in Figure S1. Prior to PDMS casting, the master mold was desiccated with TCPFOS for 1 h. PDMS and curing agent were mixed in a 10:1 ratio, poured over the master mold, and allowed to cure at 60 °C for 4 h. The PDMS replicates were then peeled from the master mold and diced into individual stamps. The stamps were coated in a 2 mM ethanolic ODT solution, and brought in contact with the Au surfaces of SPR chips (2 nm of Cr and 48 nm of Au on glass substrates) for ~15 s, leaving a patterned, self-assembled monolayer (SAM) of ODT. The SPR chips were then immersed in a previously described<sup>37</sup> Au-etching solution consisting of 1 M KOH, 0.1 M K<sub>2</sub>S<sub>2</sub>O<sub>3</sub>, 0.01 M K<sub>3</sub>Fe(CN)<sub>6</sub>, and 0.001 M K<sub>4</sub>Fe(CN)<sub>6</sub> for 20 min to remove regions of the Cr-Au film unprotected by the ODT SAM. The etching reaction was quenched by immersion of the SPR chips in fresh DI H<sub>2</sub>O. A representative schematic for the fabrication process is given in Figure S2.

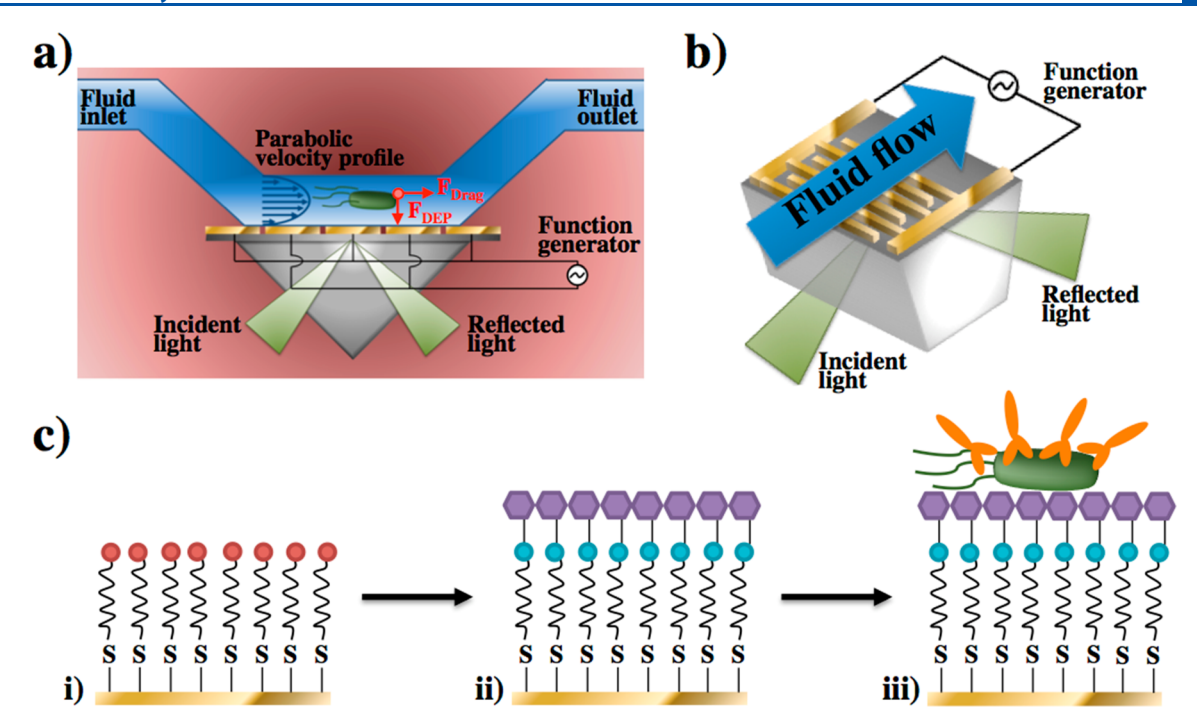


**Figure 1.** (a) Schematic illustration of the proposed DEP–SPR device. DEP-active IDEs replaced the conventional Au sensing surface (i.e., electrodeless film) in the Kretschmann SPR configuration. Alternating IDEs were connected to a function generator that established an AC potential across the IDEs and generated the necessary asymmetric electric field for DEP. The IDEs induced a dielectrophoretic force on bacterial cells that overcomes the drag force exerted by the fluid on the bacterial cells and drives bacterial mass transport to the IDE sensing surface. (b) iSPR chips were mounted such that the electrode "arms" were oriented perpendicular to the fluid flow. (c) Surface modification with DAMP and *E. coli* detection scheme: (i) 11-MUA SAMs immobilized on the surface, (ii) DAMP covalently linked to 11-MUA via EDC–NHS chemistry, and (iii) *E. coli* adsorbed on the mannosylated surface through the interaction of DAMP with the FimH adhesin of *E. coli*, followed by secondary antibody amplification.

SPR Resolution of iSPR Chips. All SPR experiments were performed with a custom-built, four-channel device that has been previously described.<sup>38</sup> Briefly, the prism-coupled instrument was constructed in the Kretschmann configuration to provide attenuated total reflection, and operated with wavelength modulation. The sensor had a wavelength resolution of 0.001 nm.<sup>39</sup> A Mylar gasket with lengths, widths, and heights of 6 mm, 3 mm, and 50  $\mu$ m, respectively, defined the four microfluidic channels. The IDEs on iSPR chips were oriented perpendicular to the direction of fluid flow (Figure S1). A peristaltic pump controlled the fluid volumetric flow rates (Ismatec, C.P. 78001-00). The length of the inlet tubing was ~22 in., causing a delay of ~5 min for the solutions to reach the sensor surface at a flow rate of 10  $\mu$ L/min. A temperature controller (ILX Lightwave, LDT-5525) was integrated into the SPR device to maintain accurate temperature control in the range of 25-40 °C. Reflectivity spectra were then collected.

Carbohydrate Surface Modification with DAMP. ODT SAMs from freshly prepared iSPR chips were removed with UV– $O_3$  cleaning for 25 min, followed by an ethanol rinse. The clean iSPR chips were immersed in a 2 mM ethanolic MUA solution for 16 h. EDC and NHS were dissolved in DI  $H_2O$  to concentrations of 400 and 40 mM, respectively. iSPR chips were removed from the MUA solution, sequentially rinsed with ethanol and DI  $H_2O$ , and dried in a stream of air. The EDC and NHS solutions were poured over the iSPR chips, which were then gently shaken for 30 min. After 30 min, the iSPR chips were rinsed with DI  $H_2O$ , immersed in a 1 mg/mL DAMP solution for 1 h, and rinsed again with DI  $H_2O$ . The iSPR chips were immersed in a 1 M glycine deactivating

solution for 30 min. Mannosylated iSPR chips were immediately used for SPR detection of *E. coli*.

**Bacterial Culture.** *E. coli* (ATCC 25922) and *S. epidermidis* (ATCC 14990) samples were received as freezedried pellets. The cell stocks made from the pellets were used throughout the study. Immediately prior to SPR characterization, cell stocks were grown to density in LB broth. A micropipettor was used to transfer  $\sim 2.5~\mu L$  of cell stock to 5 mL of LB broth, after which the cells were grown overnight at 37 °C and 250 rpm. The inoculate was added to a 250 mL Erlenmeyer flask with 50 mL of fresh LB and returned to the shaker plate in the warm room. The culture remained in the warm room for  $\sim 1~h$  until an  $OD_{600}$  of 0.6 was reached, corresponding to a concentration of  $\sim 1~\times 10^8~CFU/mL$ . The cells were rinsed by three iterations of centrifugation (15 000g for 15 min) followed by resuspension in fresh DI H<sub>2</sub>O.

**DEP–SPR Detection of** *E. coli*. Bacterial suspensions were tested immediately after being grown to an  $OD_{600}$  of  $\sim$ 0.6. Suspensions were adjusted to concentrations of  $10^3$  to  $10^8$  CFU/mL. Sensorgram baselines were established by flowing DI H<sub>2</sub>O over the conventional and iSPR chips. The volumetric flow rates for all bacterial detections were held constant at  $10 \, \mu L/\text{min}$ . Bacterial suspensions were introduced into the flow channels of the SPR instrument for 20 min, after which the flow was switched back to DI H<sub>2</sub>O for 20 min. A function generator (Instek, AFG-2225) supplied a 5  $V_{pp}$  AC voltage potential at 500 Hz across the iSPR chips, which was applied simultaneously as the inlets were switched from DI H<sub>2</sub>O to bacterial suspensions. The potential was removed when the inlets were switched back to DI H<sub>2</sub>O.

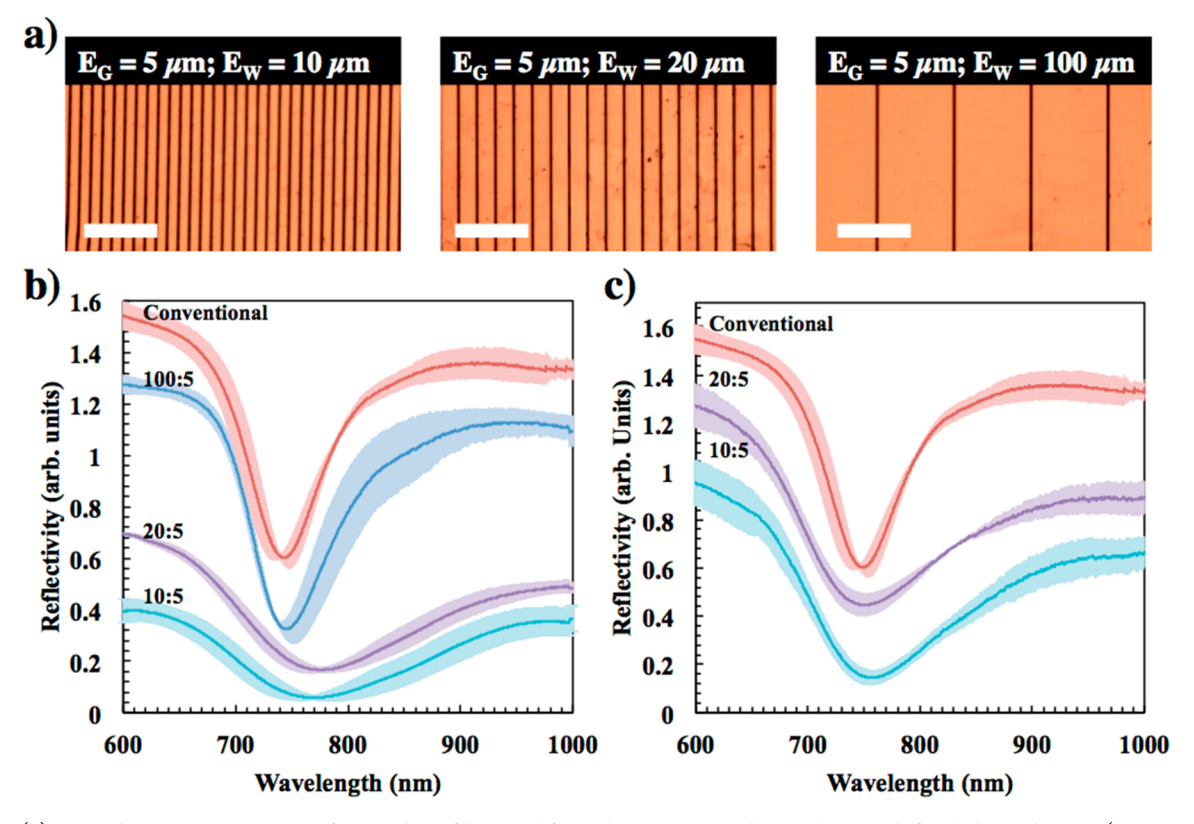


Figure 2. (a) Optical microscopy images of iSPR chips fabricated from the conventional SPR chips with fixed electrode gaps ( $E_{\rm G}=5~\mu{\rm m}$ ) and varied electrode widths ( $E_{\rm W}=10$ , 20, and 100  $\mu{\rm m}$ ). The scale bar is 100  $\mu{\rm m}$ . (b) Reflectivity of the conventional chip and iSPR chips with  $E_{\rm G}=5~\mu{\rm m}$  and  $E_{\rm W}=10$ , 20, and 100  $\mu{\rm m}$ , which were mounted with the IDEs perpendicular to the propagation of SPs. (c) Reflectivity of iSPR chips with  $E_{\rm G}=5~\mu{\rm m}$  and  $E_{\rm W}=10$  and 20  $\mu{\rm m}$ , which were rotated 90° such that the IDEs were parallel to the propagation of SPs. The error (i.e., the bands of each line) represents the standard deviations from reflectivity measurements from the four sensing channels integrated in the SPR instrument. Note that reflectivity spectra have been vertically shifted for clarity.

Selective Detection of *E. coli* with Secondary Antibody Amplification. BSA (1 mg/mL) was dissolved in PBS to block nonspecific adsorption sites, and rabbit anti-*E. coli* polyclonal antibody (PAb) was dissolved in PBS/BSA buffer at a concentration of 50  $\mu$ g/mL. After detection of *E. coli* on iSPR chips or *S. epidermidis* on conventional chips (described in the preceding section), the inlets were switched to the PBS/BSA buffer for 20 min at 10  $\mu$ L/min to reestablish the baseline. Three channels were then switched to the anti-*E. coli* PAbspiked PBS/BSA buffer for 20 min, and the fourth channel served as a reference. The inlets were switched back to the PBS/BSA buffer for 20 min to remove any unbound anti-*E. coli* PAb.

# RESULTS AND DISCUSSION

Development of DEP-Enhanced SPR System. Figure 1a shows the generalized schematic for the sensing strategy. Modifying conventional SPR chips with micrometer-sized gaps generated IDEs on iSPR chips. The asymmetrical electric fields produced by the IDEs imposed an external force on individual bacterial cells. A laminar flow with a parabolic velocity profile was established in the flow cell, which exerted a drag force on individual cells. IDEs on the iSPR chips were oriented with the electrode arms perpendicular to the fluid flow (Figure 1b). Under proper conditions, the DEP force could overcome the drag force and drive cellular adsorption on the IDE surface for detection.

IDEs with fixed electrode gaps ( $E_G = 5 \mu m$ ) and varied electrode widths ( $E_w = 10, 20, \text{ and } 100 \mu m$ ) were fabricated as

iSPR chips. IDEs enabled investigation of (1) the effect of externally applied DEP on the generation of SPs and (2) the influence of the imposed dielectrophoretic force on the mass transfer of bacterial cells during SPR-based detection. IDEs were fabricated following previously reported methods using microcontact printing<sup>37</sup> followed by wet etching.<sup>40</sup> ODT SAMs were formed on chip surfaces to investigate the comparative optical responses and inherent sensitivities of conventional and iSPR chips. For *E. coli* detection, mannosylated surfaces were used to improve cellular adsorption on conventional and iSPR chips through interaction of the FimH adhesin with surface-bound mannose, with selective detection enabled by secondary antibody amplification (Figure 1c).<sup>41,42</sup>

Effect of IDE Presence on SPR Spectral Resolution and Inherent Sensitivity. It was desired to determine how the presence of the IDEs affected the wavelength at which SPR occurred, the resolution of the SPR reflectivity spectra, and the sensitivity of the sensors. Figure 2a shows optical images of the Au IDEs on glass substrates with  $E_{\rm G}=5~\mu{\rm m}$  and  $E_{\rm w}=10$ , 20, and 100  $\mu{\rm m}$ . The reflectivity spectra for the iSPR chips with  $E_{\rm w}=10$ , 20, and 100  $\mu{\rm m}$ , which were mounted with the electrodes perpendicular to the propagation of SPs (Figure 1Sb), were collected and compared with those of a conventional SPR chip (Figure 2b). With DI H<sub>2</sub>O as the background medium, all electrodes generated SPR at the Au-H<sub>2</sub>O interface. The coupling efficiency and SP generation exhibited dependencies on  $E_{\rm w}$ . Redshifted reflectivity dips were generated at 769  $\pm$  18 and 774  $\pm$  12 nm with  $E_{\rm w}=10$  and 20  $\mu{\rm m}$ , respectively,

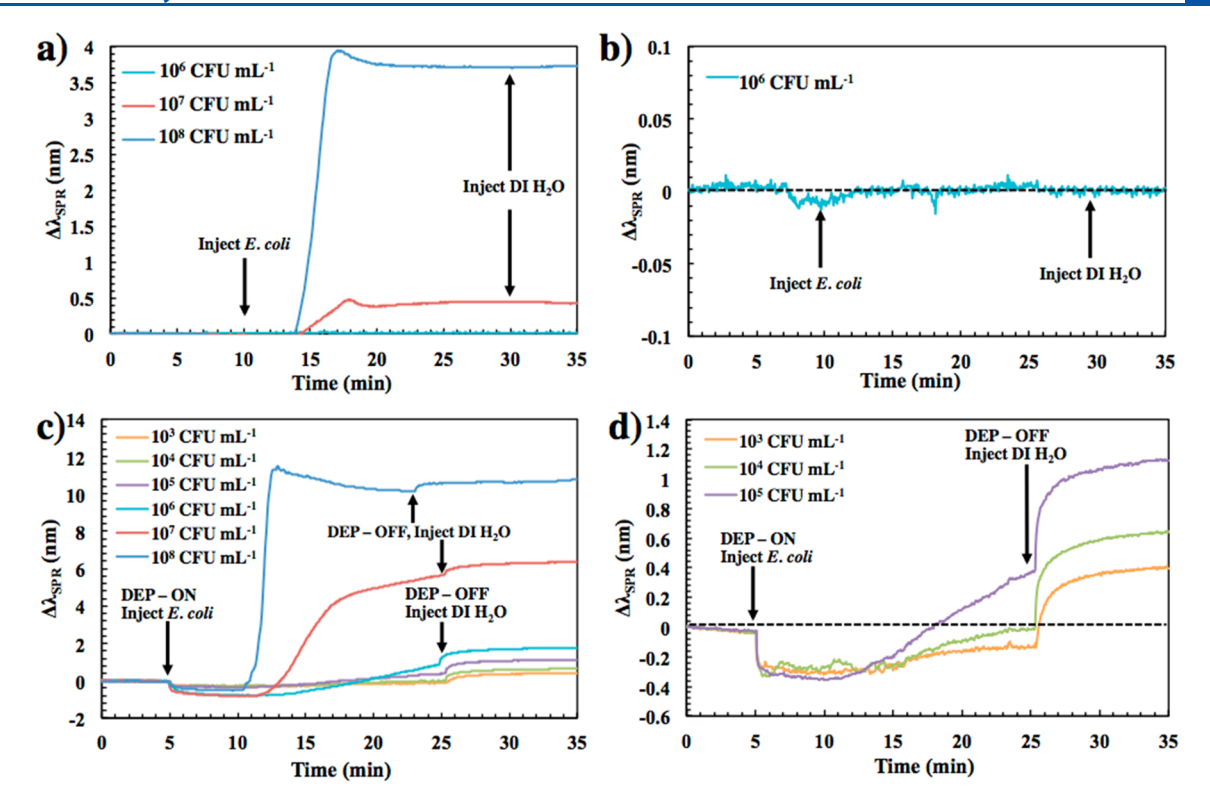


Figure 3. Sensorgrams for the real-time detection of E. coli on mannosylated (a,b) conventional SPR and (c,d) iSPR chips.

exhibiting broad and shallow reflectivity dips compared with those of the conventional SPR chip at 751  $\pm$  6 nm. As  $E_{\rm w}$  increased to 100  $\mu$ m, the reflectivity dip blueshifted to 745  $\pm$  5 nm, and drastically deepened and narrowed. The full-widths at half minimum (fwhm) for  $E_{\rm w}=$  10, 20, and 100  $\mu$ m were 147  $\pm$  15, 176  $\pm$  10, and 80  $\pm$  19 nm, respectively. The conventional chip produced a fwhm of 74  $\pm$  3 nm.

The reduced performance characteristics of iSPR chips with  $E_{\rm w}$  = 10 and 20  $\mu$ m were attributed to obstruction of SP propagation by the high densities of discontinuities in the Au films. SP propagation lengths are dependent on the metal sustaining SP excitation, the dielectric medium directly above the metal, and the wavelength of the incident light. The propagation lengths of SPs generated at the Au-H2O interfaces ranged from 3-24  $\mu$ m in the 630-850 nm spectral window. 10 Therefore, it was speculated that the high densities of discontinuities in the Au films on iSPR chips with  $E_{\rm w} = 10$ and 20 µm prevented efficient SP propagation and resulted in poor resolution of the reflectivity spectra. iSPR chips with  $E_{\rm w}$  = 10 and 20  $\mu$ m are therefore rendered nonviable for SPR sensing as the resolution for wavelength-modulated SPR sensors are dependent on how accurately the reflectance dip can be monitored with the local change in refractive index.

To further explore the SPR resolution of iSPR chips ( $E_{\rm w}=10$  and 20  $\mu{\rm m}$ ) with respect to the length of SP propagation, the iSPR chips were rotated 90° such that the Au electrode arms were oriented in the direction of SP propagation. As seen in Figure 2c, the reflectivity spectra of IDEs rotated 90° displayed smaller deviations from the reflectivity spectrum of the conventional device. The orientation-dependent reflectivity spectra show that the impediment of SP propagation was due to the discontinuous Au film.

The inherent sensitivity of the iSPR ( $E_G = 5 \mu m$  and  $E_w = 100 \mu m$ ) chips with respect to bulk-refractive-index changes

was investigated and compared to that of the conventional chip. Detailed experimental procedures are given in the SI. Figure S3 shows that the sensitivities of the conventional and iSPR chips were 6103 and 6104 nm/RIU, respectively. Therefore, the discontinuities present in the iSPR chips did not reduce sensing performance.

DEP-Enhanced SPR Detection of E. coli. The detection sensitivities toward E. coli suspensions for conventional and iSPR chips were directly compared. The dielectrophoretic force exerted on an E. coli cell was estimated theoretically (see the SI for details). As shown in Figure S4, nonconductive media, such as DI  $H_2O$  with low medium conductivity ( $\sigma_m$  = 10<sup>-4</sup> S/m), produces the largest pDEP force in the lowfrequency regime. Therefore, the applied potential was held constant at 500 Hz and 5  $V_{pp}$  (peak-to-peak voltage) for the duration of the DEP-SPR experiments to ensure a maximal pDEP force. The Au surfaces of conventional and iSPR chips were first mannosylated, as the LOD for conventional chips was extraordinarily high (108 CFU/mL), using a simple octadecanethiol SAM (Figure S5). E. coli containing type-1 fimbriae express the FimH adhesin, which recognizes and adheres to highly mannosylated surfaces. 41,42 Highly mannosylated surfaces have been previously employed in SPR biosensing, and showed drastically increased cellular adherence to the SPR-sensing surface.<sup>43</sup>

Figure 3a shows the results for *E. coli* detection with the conventional SPR chip. SPR-wavelength shifts  $(\Delta \lambda_{\rm SPR})$  of  $3.734 \pm 0.009$  and  $0.429 \pm 0.017$  nm were observed for *E. coli* concentrations of  $10^8$  and  $10^7$  CFU/mL, respectively. Reduction in the bacterial concentration to  $10^6$  CFU/mL produced no observable shift in  $\Delta \lambda_{\rm SPR}$  (Figure 3b).

For *E. coli* detection with the iSPR chip, DEP was applied simultaneously as the inlets were switched from DI  $H_2O$  to the bacterial suspensions. Immediately, a negative  $\Delta \lambda_{SPR}$  was

observed. The negative SPR-wavelength shift was attributable to localized temperature increases in the vicinity of the IDEs that change the refractive index of DI H<sub>2</sub>O (see the details in SI). The negative shift was found to be dependent on the AC voltage applied, but independent of volumetric flow rate (Figure S6a). The temperature increase with DEP application was estimated to be ~0.5 °C (Figure S6b), indicating that the bacterial cells would experience no temperature-induced conformational changes or thermal stress. Approximately 5 min after DEP application, the bacterial suspensions reached the IDE surfaces through the tubes from the inlets and were drawn to the surface through pDEP, leading to positive shifts in  $\Delta \lambda_{SPR}$  (Figure 3c). The slope of the temporal response was concentration-dependent, with the most concentrated suspension (108 CFU/mL) producing the steepest slope. Compared with the performance of the conventional chip,  $\sim 15$ - and  $\sim 3$ fold increases in  $\Delta \lambda_{SPR}$  for the iSPR chip were observed for the  $10^7$  and  $10^8$  CFU/mL bacterial suspensions, respectively. Furthermore, the iSPR chip was able to resolve shifts in  $\Delta \lambda_{\text{SPR}}$ in dilute E. coli suspensions as low as 10<sup>3</sup> CFU/mL (Figure 3d). Upon the first application of DEP, the negative  $\Delta \lambda_{SPR}$  was clearly visible, but it increased rapidly when bacterial cells began flowing over the IDEs. Removal of the 5 V<sub>pp</sub> potential resulted in a rapid increase in  $\Delta \lambda_{SPR}$  as the local temperature near the IDEs was speculated to have decreased. The total compensated shift in  $\Delta \lambda_{SPR}$  for  $10^3$  CFU/mL was found to be  $0.619 \pm 0.016$  nm. Figure 4 shows the comparative plot of the SPR-sensing performances of the conventional and iSPR chips as functions of E. coli concentration.

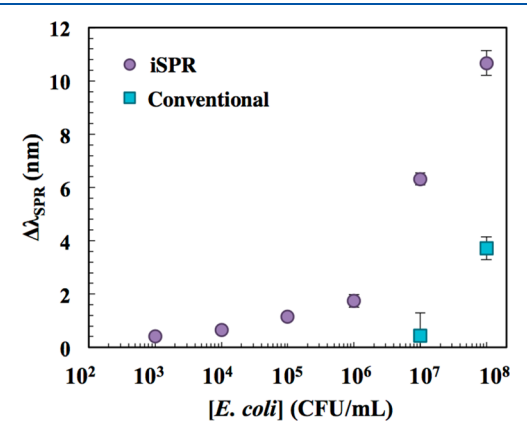


**Figure 4.** SPR-wavelength shifts of the conventional and iSPR chips as functions of  $E.\ coli$  concentration. Error bars represent  $3\times$  the standard deviation of the steady-state SPR-wavelength shift.

The LOD in SPR biosensing is commonly defined as the  $\Delta\lambda_{\rm SPR}$  equal to 3× the standard deviation of the noise of the reference channel. The DI H<sub>2</sub>O baseline was used to define the noise of 0.141 nm. The DEP–SPR data were fit to a linear model, and the LOD for the iSPR chip was determined to be ~3.0 × 10² CFU/mL. Therefore, the increased cell flux to the IDEs induced by DEP led to a nearly 5 order of magnitude improvement in the LOD of the iSPR chip compared with that of the conventional chip. The greatly improved LOD makes this sensing method have broader applications, such as the biomedical diagnosis of urinary-tract infections, which require the detection of bacteria in concentrations as low as  $10^3$  CFU/mL.  $^{6-8}$ 

Selective Detection of *E. coli* with Antibody-Based Secondary Amplification. To further amplify the SPR responses as well as to enable selective detection, anti-*E. coli* polyclonal antibodies (PAb) were used, and *S. epidermidis* was selected to serve as nontarget bacteria. Figure 5a shows the

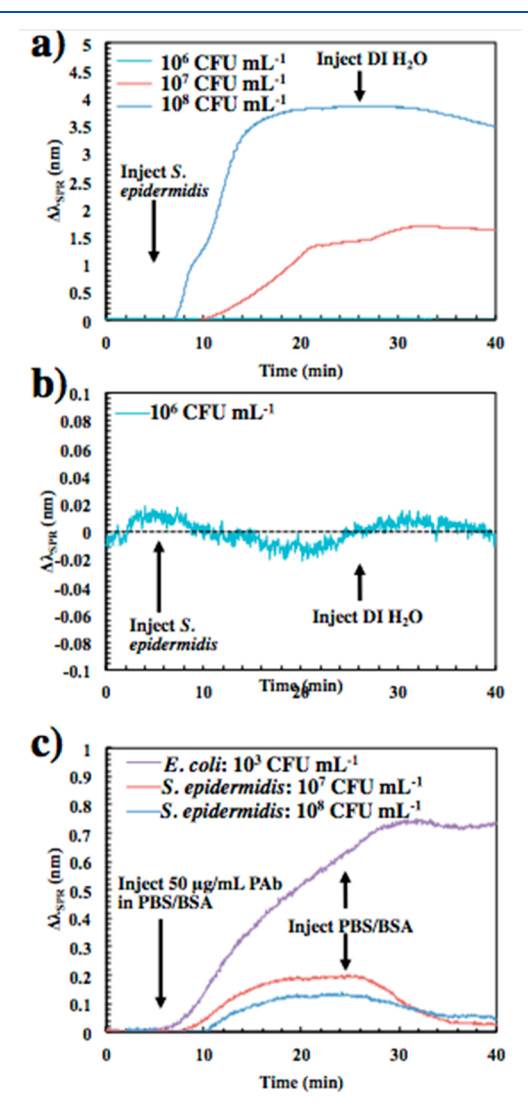


**Figure 5.** (a) Sensorgrams of the response to *S. epidermidis* suspensions ranging in concentration from  $10^6$  to  $10^8$  CFU/mL in DI  $\rm H_2O$  on a mannosylated conventional SPR chip. (b) Expanded view of the  $10^6$  CFU/mL *S. epidermidis* suspension, showing no response. (c) Sensorgrams of secondary PAb amplification of the  $10^7$  and  $10^8$  CFU/mL *S. epidermidis* suspensions in (a) and the  $10^3$  CFU/mL *E. coli* suspension captured with DEP in Figure 3d. The entire sensorgrams for each concentration of bacteria are shown in Figure S7.

SPR response to *S. epidermidis* on the mannosylated conventional chip. Similar to *E. coli*, the  $10^7$  and  $10^8$  CFU/mL *S. epidermidis* suspensions caused shifts in  $\Delta \lambda_{\rm SPR}$  of  $1.621 \pm 0.029$  and  $3.502 \pm 0.101$  nm, respectively, whereas no response was observed for the  $10^6$  CFU/mL suspension (Figure 5b).

After immobilization of 10<sup>7</sup> and 10<sup>8</sup> CFU/mL *S. epidermidis* suspensions on a mannosylated conventional chip (Figure 5a) and a 10<sup>3</sup> CFU/mL *E. coli* suspension on a mannosylated iSPR chip (Figure 3d), the adsorbed bacteria were exposed to anti-*E. coli* PAb. A PBS/BSA buffer solution was flowed through the

channels to block nonspecific-adsorption sites on the chips prior to flowing 50 µg/mL anti-E. coli PAb in the PBS/BSA buffer solution. The net shifts in  $\Delta \lambda_{SPR}$  for the 10<sup>7</sup> and 10<sup>8</sup> CFU/mL S. epidermidis suspensions were 0.028 ± 0.003 and  $0.053 \pm 0.004$  nm, respectively (Figure 5c). The negligible increase in  $\Delta \lambda_{SPR}$  for the anti-E. coli PAb secondary amplification of S. epidermidis indicates the lack of interaction of S. epidermidis with anti-E. coli PAb. Conversely, E. coli exhibited nonreversible binding to anti-E. coli PAb and a stable increase in  $\Delta \lambda_{SPR}$  of 0.741  $\pm$  0.054 nm upon secondary amplification for the 10<sup>3</sup> CFU/mL E. coli suspension (Figure 5c). The complete sensorgrams for the 10<sup>7</sup> and 10<sup>8</sup> CFU/mL S. epidermidis suspensions on a mannosylated conventional SPR chip and for the 10<sup>3</sup> CFU/mL E. coli suspension on a mannosylated iSPR chip are shown in Figure S7. The secondary-amplification demonstrates that dilute (10<sup>3</sup> CFU/ mL) suspensions of target bacteria can be selectively detected in the presence of nontarget bacteria with iSPR chips. Multifunctional coatings, that incorporate nonfouling elements and highly selective biorecognition elements have enabled bacterial detection in complex matrices. 44-46 Synergistic effects between multifunctional coatings and the DEP-enhanced approach presented here could lead to further improvements in SPR-based bacterial detection.

## CONCLUSION

In this work, the integration of dually functional IDEs capable of sustaining SPR and generating DEP into a single iSPR chip was investigated. SP generation was found to be dependent on the presence of discontinuities in the Au films used to define the widths of the IDEs. IDEs with widths greater than the SP propagation length were found to sustain sharp reflectivity dips comparable to those of the conventional SPR device. The inherent sensitivity to changes in the bulk refractive index of the iSPR chip were found to be nearly identical to those of the conventional chip, indicating that the 5  $\mu m$  electrode gaps did not introduce detrimental sensitivity side effects.

The iSPR chip was used to improve the LOD of E. coli by nearly 5 orders of magnitude with the application of DEP, compared with that of the conventional SPR chip without DEP. The LOD for the iSPR chip was found to be  $\sim 3.0 \times 10^2$ CFU/mL, compared with  $\sim 1 \times 10^7$  CFU/mL for the conventional SPR chip. The improved LOD in the iSPR chip was attributed to increased mass transport of bacterial cells to the IDE surface. Unlike conventional SPR chips that rely solely on the diffusion of cells to the sensing surface, iSPR chips increase cellular accumulation on the IDE surface through the addition of DEP driving force. Furthermore, selective detection of E. coli over nontarget S. epidermidis was enabled through secondary antibody amplification. Secondary antibody amplification generated additional SPR shifts for dilute (10<sup>3</sup> CFU/mL) E. coli, whereas the S. epidermidis signals of concentrated suspensions (107 and 108 CFU/mL) were unamplified. The strategy developed here demonstrates that the integration of DEP and SPR into a bacterial-detection module can enable sensitive detection of dilute bacterial suspensions, and when combined with downstream antibody amplification, it can discriminate target from nontarget bacteria. Further functionalization of the sensing surface with nonfouling materials could offer a promising method for rapid, sensitive, and specific detection of bacteria in complex media with broad applications in the areas of biomedical diagnostics, environmental monitoring, food safety, and homeland security.

#### ASSOCIATED CONTENT

# S Supporting Information

The Supporting Information is available free of charge on the ACS Publications website at DOI: 10.1021/acs.analchem.8b05137.

Schematic of IDE dimensions, schematic of fabrication protocol, comparison of conventional and iSPR chips in terms of bulk-refractive-index changes, CM-factor calculations for *E. coli* and DEP-force potential, sensorgrams comparing responses to *E. coli* adsorption on ODT and mannose-functionalized surfaces, sensorgrams comparing SPR responses of DEP and temperature variations, and complete sensorgrams for the adsorption and selective detection of *E. coli* and *S. epidermidis* (PDF)

## AUTHOR INFORMATION

#### **Corresponding Author**

\*Tel.: +1-206-543-4807. E-mail: qyu@uw.edu.

#### ORCID ®

Daniel David Galvan: 0000-0001-6282-6156

Erik Liu: 0000-0003-4775-2544 Qiuming Yu: 0000-0002-2401-4664

#### Notes

The authors declare no competing financial interest.

#### ACKNOWLEDGMENTS

The authors gratefully acknowledge financial support provided by the National Science Foundation (NSF, CMMI 1661660). We also would like to thank Duane Irish at the Washington Nanofabrication Facility (WNF) for fabrication of the silicon master mold. The WNF is part of the National Nanotechnology Coordinated Infrastructure (NNCI) at the University of Washington supported by the NSF (ECCS-1542101).

# REFERENCES

- (1) Levy, S. B. Sci. Am. 1998, 278 (3), 46-53.
- (2) Levy, S. B.; Marshall, B. Nat. Med. 2004, 10 (12), S122-S129.
- (3) Haley, R. W.; Culver, D. H.; White, J. W.; Morgan, W. M.; Emori, T. G. Am. J. Epidemiol. 1985, 121 (2), 159–167.
- (4) Weinstein, R. A. Emerging Infect. Dis. 1998, 4 (3), 416-420.
- (5) Marston, H. D.; Dixon, D. M.; Knisely, J. M.; Palmore, T. N.; Fauci, A. S. *JAMA* **2016**, *316* (11), 1193–1204.
- (6) Nicolle, L. E.; Bradley, S.; Colgan, R.; Rice, J. C.; Schaeffer, A.; Hooton, T. M. Clin. Infect. Dis. 2005, 40 (5), 643–654.
- (7) Hooton, T. M. N. Engl. J. Med. 2012, 366 (11), 1028-1037.
- (8) Avci, E.; Kaya, N. S.; Ucankus, G.; Culha, M. Anal. Bioanal. Chem. 2015, 407 (27), 8233–8241.
- (9) Homola, J. Chem. Rev. 2008, 108 (2), 462-493.
- (10) Homola, J.; Yee, S. S.; Gauglitz, G. Sens. Actuators, B **1999**, 54 (1–2), 3–15.
- (11) Taylor, A. D.; Ladd, J.; Yu, Q. M.; Chen, S. F.; Homola, J.; Jiang, S. Y. Biosens. Bioelectron. 2006, 22 (5), 752-758.
- (12) Vaisocherova-Lisalova, H.; Visova, I.; Ermini, M. L.; Springer, T.; Song, X. C.; Mrazek, J.; Lamacova, J.; Lynn, N. S.; Sedivak, P.; Homola, J. *Biosens. Bioelectron.* **2016**, *80*, 84–90.
- (13) Farka, Z.; Jurik, T.; Pastucha, M.; Skladal, P. Anal. Chem. 2016, 88 (23), 11830–11836.
- (14) Vala, M.; Etheridge, S.; Roach, J. A.; Homola, J. Sens. Actuators, B **2009**, 139 (1), 59–63.
- (15) Huang, C. J.; Dostalek, J.; Sessitsch, A.; Knoll, W. Anal. Chem. **2011**, 83 (3), 674–677.

(16) Huang, C. J.; Knoll, W.; Sessitsch, A.; Dostalek, J. *Talanta* **2014**, 122, 166–171.

- (17) Gervais, T.; Jensen, K. F. *Chem. Eng. Sci.* **2006**, *61* (4), 1102–1121.
- (18) Wang, Y.; Knoll, W.; Dostalek, J. Anal. Chem. 2012, 84 (19), 8345-8350.
- (19) Ruppel, N.; Troger, V.; Sandetskaya, N.; Kuhlmeier, D.; Schmieder, S.; Sonntag, F. Eng. Life Sci. 2018, 18 (4), 263–268.
- (20) Liu, X.; Hu, Y. X.; Zheng, S.; Liu, Y.; He, Z.; Luo, F. Sens. Actuators, B 2016, 230, 191–198.
- (21) Pohl, H. A. J. Appl. Phys. 1951, 22 (7), 869-871.
- (22) Pethig, R. Biomicrofluidics 2010, 4 (2), 022811.
- (23) Hamada, R.; Takayama, H.; Shonishi, Y.; Mao, L.; Nakano, M.; Suehiro, J. Sens. Actuators, B 2013, 181, 439–445.
- (24) Kim, M.; Jung, T.; Kim, Y.; Lee, C.; Woo, K.; Seol, J. H.; Yang, S. *Biosens. Bioelectron.* **2015**, *74*, 1011–1015.
- (25) del Moral-Zamora, B.; Punter-Villagrassa, J.; Oliva-Branas, A. M.; Alvarez-Azpeitia, J. M.; Colomer-Farrarons, J.; Samitier, J.; Homs-Corbera, A.; Miribel-Catala, P. L. *Electrophoresis* **2015**, *36* (9–10), 1130–1141.
- (26) Couniot, N.; Francis, L. A.; Flandre, D. Lab Chip 2015, 15 (15), 3183-3191.
- (27) Braff, W. A.; Willner, D.; Hugenholtz, P.; Rabaey, K.; Buie, C. R. PLoS One **2013**, 8 (10), No. e76751.
- (28) Park, S.; Zhang, Y.; Wang, T. H.; Yang, S. Lab Chip 2011, 11 (17), 2893–2900.
- (29) Yang, L. J. Talanta 2009, 80 (2), 551-558.
- (30) Schroder, U. C.; Ramoji, A.; Glaser, U.; Sachse, S.; Leiterer, C.; Csaki, A.; Hubner, U.; Fritzsche, W.; Pfister, W.; Bauer, M.; Popp, J.; Neugebauer, U. Anal. Chem. 2013, 85 (22), 10717–10724.
- (31) Schroder, U. C.; Beleites, C.; Assmann, C.; Glaser, U.; Hubner, U.; Pfister, W.; Fritzsche, W.; Popp, J.; Neugebauer, U. Sci. Rep. 2015, 5, No. 8217.
- (32) Zhang, P. R.; Ren, L. H.; Zhang, X.; Shan, Y. F.; Wang, Y.; Ji, Y. T.; Yin, H. B.; Huang, W. E.; Xu, J.; Ma, B. *Anal. Chem.* **2015**, *87* (4), 2282–2289.
- (33) Cheng, I. F.; Chang, H. C.; Hou, D.; Chang, H. C. Biomicrofluidics 2007, 1 (2), 021503.
- (34) Cheng, I. F.; Lin, C. C.; Lin, D. Y.; Chang, H. Biomicrofluidics **2010**, *4* (3), 034104.
- (35) Cheng, I. F.; Chang, H. C.; Chen, T. Y.; Hu, C. M.; Yang, F. L. Sci. Rep. 2013, 3, No. 2365.
- (36) Cheng, I. F.; Chen, T. Y.; Lu, R. J.; Wu, H. W. Nanoscale Res. Lett. 2014, 9, 324.
- (37) Qin, D.; Xia, Y.; Whitesides, G. M. Nat. Protoc. 2010, 5 (3), 491–502.
- (38) Boozer, C.; Yu, Q. M.; Chen, S. F.; Lee, C. Y.; Homola, J.; Yee, S. S.; Jiang, S. Y. Sens. Actuators, B **2003**, 90 (1-3), 22-30.
- (39) Vaisocherova, H.; Faca, V. M.; Taylor, A. D.; Hanash, S.; Jiang, S. Y. Biosens. Bioelectron. **2009**, 24 (7), 2143–2148.
- (40) Xia, Y. N.; Zhao, X. M.; Kim, E.; Whitesides, G. M. Chem. Mater. 1995, 7 (12), 2332-2337.
- (41) Barshavit, Z.; Goldman, R.; Ofek, I.; Sharon, N.; Mirelman, D. Infect. Immun. 1980, 29 (2), 417–424.
- (42) Bouckaert, J.; Mackenzie, J.; de Paz, J. L.; Chipwaza, B.; Choudhury, D.; Zavialov, A.; Mannerstedt, K.; Anderson, J.; Pierard, D.; Wyns, L.; Seeberger, P. H.; Oscarson, S.; De Greve, H.; Knight, S. D. Mol. Microbiol. 2006, 61 (6), 1556–1568.
- (43) Yazgan, I.; Noah, N. M.; Toure, O.; Zhang, S. Y.; Sadik, O. A. *Biosens. Bioelectron.* **2014**, *61*, 266–273.
- (44) Zhang, X.; Tsuji, S.; Kitaoka, H.; Kobayashi, H.; Tamai, M.; Honjoh, K.; Miyamoto, T. *J. Food Sci.* **2017**, 82 (10), 2357–2363.
- (45) Templier, V.; Livache, T.; Boisset, S.; Maurin, M.; Slimani, S.; Mathey, R.; Roupioz, Y. Sci. Rep. 2017, 7, No. 9457.
- (46) Helali, S.; Alataw, A. S. E.; Abdelghani, A. *J. Food Saf.* **2018**, 38 (5), e12510.